Sensitivity Analysis of Global Kinematics on Mantle Structure Using Automatically Generated Adjoint Thermochemical Convection Codes

N. Coltice[1] S. Blessing[2] R. Giering[2] P.J. Tackley[3]

[1] Laboratoire de Géologie, Ecole Normale Supérieure, PSL Res. Univ., Paris, France.

[2] FastOpt, Germany

[3] Institute of Geophysics, Department of Earth Sciences, ETH Zurich, Switzerland

Sensitivity Analysis of Global Kinematics on Mantle Structure Using Automatically Generated Adjoint Thermochemical Convection Codes

N. Coltice[1] S. Blessing[2] R. Giering[2] P.J. Tackley[3]

[1] *Laboratoire de Géologie, Ecole Normale Supérieure, PSL Res. Univ., Paris, France.*

[2] *FastOpt, Germany*

[3] *Institute of Geophysics, Department of Earth Sciences, ETH Zurich, Switzerland*

SUMMARY

Within the past 30 years, numerical models of mantle convection have been able to predict observations on Earth and planets, and among them tectonics. The possibility of building inverse problems in global geodynamics became concrete, and often involve the development of adjoint codes. Such tools provide efficient ways to estimate sensitivities of misfit functions relative to control parameters, like errors on predicted velocities relative to mantle 3D structure. One issue to build an adjoint code is that such code is problem specific in many cases, while forward codes are versatile. We propose here a way to build adjoint codes that are exact adjoints of forward codes through an automated process. Using the automatic differentiation translator TAF (Giering and Kaminski (2003)) and incorporating specific implementations for MPI communications, we generate two adjoint codes of the 3D spherical thermomechanical mantle convection code StagYY (Tackley (2008)). We first present a benchmarking example computing the sensitivities of a thermal state to initial conditions with a 3D spherical thermochemical model. We then compute the sensitivities of present-day plate velocities relative to guessed temperature distribution in the mantle. The sensitivities reflect either the intrinsic sensitivity of the problem (sensitivity to upper mantle structure) and the errors made in reconstructing the thermal structure of the mantle (deepest mantle structure). Both codes successfully pass the rigorous and demanding gradient test, also called Taylor test. We show that our workflow for automatic generation of adjoint codes for StagYY provides a sustainable and adaptive method to engage in inverse modelling and sensitivity computations of 3D global geodynamics.

Key words: Adjoint, Automatic differentiation, inverse methods, mantle convection

1 INTRODUCTION

Modelling the flow within planetary mantles remains a horizon limited by both modelling capabilities (theory, experiments and computers) and observations. Quantitatively describing the link between what we observe at the surface of planets through geological mapping, geophysical probing, on one side, and geochemical databases, on the other side, faces challenges: building dynamic models that are predictive enough and inverse methods capable of dealing with complex models and both heterogeneous and sparse databases. In the past 20 years, geodynamic models of mantle convection and lithosphere dynamics have made a leap forward by including 3D fine resolution, multi-physics and more appropriate rock rheologies (Tackley (2012)). Therefore, they became more and more predictive for fundamental aspects of Earth's geology and geophysics (Tackley (2000); Coltice et al. (2017)).

In the late 1990's beowulf computer clusters took mantle convection to a new stage: it was possible to generate 3D spherical models at high convective vigor although rheological approximations were crude (Bunge et al. (1996)). Capitalizing on geodynamics of the 1980's, a generation of models used tectonic plate kinematics as surface boundary conditions (Bunge et al. (2000); Zhong et al. (2000)). They predicted the large-scale temperature field that could be compared with tomographic models that had also made decisive progress at the time (Grand et al. (1997)). (Bunge et al. (2003)) proposed an inverse methodology with these forced models, using the tomographic images as the target quantity and 3D temperature field in the past as the control variable. The goal was to retrieve the 3D thermal history of the mantle through the Cenozoic. The method relies on an adjoint code, which provides in one step the sensitivity of a misfit function to the full set of control variables (Talagrand (1997)). In order to realise an inversion, both forward and adjoint code have to be embeded with a minimisation scheme. In (Bunge et al. (2003)), the adjoint code was built by solving adjoint equations with similar solvers as the forward code, neglecting the treatment of strong lateral viscosity variations or stress-dependent rheologies. The same year, (Ismail-Zadeh et al. (2003)) also proposed an inverse approach to a similar inverse problem, solving the adjoint equation for temperature and accounting for pressure and temperature dependent viscosity in the inversion scheme. This work was further developed in a subsequent paper (Ismail-Zadeh et al. (2004)). This was a first step for a lineage of studies (Liu and Gurnis (2008); Liu et al. (2008); Ghelichakhan and Bunge (2018); Colli et al. (2018)). Initial thermal conditions and rheological parameters are the two ingredients for predicting a geodynamical evolution (initial chemical composition could also be considered). The latter has been the focus of inverse methods in lithosphere modeling using surface deformation, stresses and gravity as targets (Baumann et al. (2014); Reuber et al. (2020)).

In the past 10 years, the parameterisation of 3D spherical models of mantle convection improved to generate surface tectonics self-consistently, which opened the way to study global tectonics and thermal mantle structure together (Crameri et al. (2014); Coltice et al. (2019)). The recipe relies on a rheological approximation of mechanical properties of rocks. Exponential temperature-dependent viscosity allows a strong lid to form as long as viscosity contrats are larger than 10^3. Combining it with a yield stress formulation generates strain localization on narrow boundaries and a strong toroidal velocity component (Tackley (2000)). Such models produce Earth's like area-age distributions (Coltice et al. (2012)), plate size distributions (Mallard et al. (2016)), supercontinent cycles (Rolf et al. (2014)), transform-like structure (Langemeyer et al. (2021)), plate reorganizations (Coltice et al. (2019)), and hotspot properties (Arnould et al. (2020)). Capitalizing on the forecasting behavior of these models (Coltice and Shephard (2018)), two groups have developed inverse methods targeting surface observations to unravel deep properties. (Bocher et al. (2016); Bocher et al. (2018)) proposed Bayesian data assimilation strategies to infer the internal temperature evolution from heat flow and kinematics at the surface in synthetic 2D models. These Kalman filter methods employ the forward convection code and exploit statistical properties of convective flows to fit the data. (Worthen et al. (2014); Ratnaswamy et al. (2015); Li et al. (2017)) have proposed adjoint-based strategies to evaluate quantitatively the trade-off between rheology and internal temperature when fitting surface kinematics. They solve adjoint equations in 2D models focused on subduction.

An adjoint code is built by differentiating the forward code and reversing the chain rule of elementary actions (Talagrand (1991); Talagrand (1997)). Changing the target quantities and/or the control variable means that each new geodynamic inverse problem requires its specific adjoint code development, although the forward code remains the same. The core of the adjoint code can however be very similar if two problems involving the exact same control variables. The loss of versatility of adjoint codes relative to forward codes can restrict the variety of geodynamic problems to be studied. Therefore, we propose here a framework for automatically generating and maintaining adjoint codes for multi-geometry, multi-physics convection code StagYY (Tackley (2008)). We adapt the forward code StagYY and the automatic differentiation translator TAF (Giering and Kaminski (2003)) to generate tangent linear and adjoint codes. We describe here the methodology and realise an exacting benchmarking (ensuring that the adjoint code is the exact adjoint of the forward code) with gradient tests on 3D spherical thermochemical convection cases with and without non-linear rheology. We do not realise here inversions here but rather focus on the evaluation of outcomes of adjoint codes. We compute the sensitivities of plate velocities to the 3D temperature field in a mantle flow model with plate-like behavior. We explore how sensitivities depend on the guessed temperature distribution in the mantle and rheological parameters.

2 THE FORWARD MANTLE CONVECTION CODE: STAGYY

2.1 30 years of StagYY code development

The simulation code StagYY originated in 1992 and has been expanded and enhanced since then. Originally called Stag3D and written in Fortran 77 to model infinite Prandtl number, variable-viscosity convection in 3D Cartesian geometry, the first resulting publication was (Tackley (1993)). Subsequently, Stag3D was enhanced to include phase transitions (Tackley (1996)) and to track chemical variations using a marker-in-cell technique (Tackley (1998)). It was used to produce some of the first 3D models of self-consistent plate tectonics, using strain-rate-weakening or plastic rheology (Tackley (1998); Tackley (2000)). Next, two-dimensional cylindrical geometry was added as an option, as were the abilities to model melting-induced chemical differentiation (Xie and Tackley (2004)) and couple core evolution to the mantle (Nakagawa and Tackley (2004))

Stag3D was transformed into StagYY by converting to Fortran 90 and adding 3-D spherical geometry (Tackley (2008)). A new 2-D spherical approximation, the spherical annulus, was also implemented (Hernlund and Tackley (2008)). Subsequent enhancements include coupling to plate motion histories (Bello et al. (2015)), visco-elasticity (Patočka et al. (2017)), a more advanced melting treatment that can produce continental crust in addition to the previously-implemented oceanic crust (Jain et al. (2019)) and multiple impacts (Borgeat and Tackley (2022)). StagYY has been applied to model Earth and various planets including including Mars (Keller and Tackley (2009)), Venus (Armann (2012)) and super-Earths (Tackley et al. (2014)).

Besides the benchmarking of the code presented in some of the publications cited above, such as (Tackley (2008)), StagYY was part of community benchmarking initiatives (Crameri et al. (2011); Tosi et al. (2015)).

2.2 Equations

The truncated anelastic approximation is assumed (see details in (Tackley (2008)) and (Ricard et al. (2022))) for more on compressibility approximations, leading to the following set of equations for conservation of mass:

$$\nabla \cdot (\bar{\rho}\mathbf{v}) = 0, \tag{1}$$

momentum

$$\nabla \cdot \underline{\underline{\sigma}} - \nabla p = \rho \vec{g}, \tag{2}$$

and energy

$$\rho C_p \frac{DT}{Dt} = -\bar{\alpha}\bar{\rho}T v_r + \nabla \cdot (k\nabla T) + \bar{\rho}H + \underline{\underline{\sigma}} : \underline{\underline{\dot{e}}}, \tag{3}$$

where $\mathbf{v}$ is velocity, v_r being the radial component, p is pressure, $\underline{\underline{\sigma}}$ is the deviatoric stress tensor and $\underline{\underline{\dot{e}}}$ the strain-rate tensor (the latter two are given by standard expressions in Cartesian or spherical polar coordinates with variable viscosity), and physical properties are density ρ, gravitational acceleration vector $\vec{g}$, specific heat capacity C_p, thermal expansivity α, thermal conductivity k and internal heating rate H. Overbars denote reference state properties that are dependent on depth only. StagYY can be run using either dimensional or non-dimensional units, in which case the physical properties are relative to reference values and the Rayleigh number is incorporated into the right-hand side of the momentum equation (see (Tackley (2008))); further to this, the Boussinesq approximation allows for setting all material properties except viscosity equal to 1 and deleting the adiabatic heating and viscous dissipation terms in the energy equation (the first and last terms on the right-hand side, respectively).

Probably the most important physical property is viscosity, which appears in the stress expression and can vary by many orders of magnitude. In StagYY it can be dependent on temperature, pressure, stress, composition, and accumulated strain, with choices of viscosity laws for these various dependencies.

When compositional variations are tracked, the following must be satisfied:

$$\frac{DC_i}{Dt} = 0 \tag{4}$$

where C_i is the fraction of compositional component i.

Partial melting is also implemented, as well as melt-solid segregation and intrusive and extrusive magmatism. For details of the latest treatment see (Jain et al. (2019)).

2.3 Numerical methods

A finite volume discretization is used, with velocity components and pressure defined on a staggered grid (Patankar(1980); Ogawa et al. (1991)). Both cartesian and spherical grids are implemented, and in both two and three dimensions. For three-dimensional spherical geometry covering a complete sphere, the yin-yang spherical grid is used (Kageyama and Sato (2004)), which covers the sphere using two overset patches similar to the construction of a tennis ball - here the minimum overlap version is used. For two-dimensional spherical geometry, the spherical annulus geometry is used (Hernlund and Tackley (2008)).

The momentum and pressure equations are solved simultaneously using either a geometric multi-grid solver or (in 2-D) a choice of direct solvers. In the case of nonlinear rheology (plasticity or dislocation creep), Picard iterations are used to converge on the correct viscosity. The energy equation is time-stepped explicitly.

Tracers (markers) are used to track compositional information, both for bulk composition and trace-element composition, and may optionally also track temperature and/or viscosity. They are advected using a 4th-order Runge-Kutta method. See (Tackley and King (2003)).

2.4 Implementation

StagYY is written in Fortran using features introduced up to Fortran 2013. It may be compiled in isolation, or linked to one or more libraries, the main ones being MPI (for parallelisation), HDF5 (for input/output), and PETSc, MUMPS and UMFPACK (for direct solvers). Parallelisation uses a three-dimensional domain decomposition; when using the yin-yang grid the maximum azimuthal decomposition is currently limited to 8 ways.

3 AUTOMATIC GENERATION OF ADJOINT CODE OF STAGYY

3.1 Principles of automatic differentiation

Algorithmic Differentiation (AD), also known as Automatic Differentiation, holds significant potential for geodynamicists seeking to analyze derivatives in the context of their algorithms, such as those embedded in software like StagYY. This technique enables the computation of function derivatives (for instance the sensitivity of the difference between plate velocities and those predicted by a geodynamic model as a function of the 3D temperature field) directly from algorithmic source code. The core concept of AD rests on recognizing that even the most intricate algorithms can be deconstructed into a sequence of elementary operations. These operations, which manipulate numerical values, can be differentiable, yielding local Jacobian information (Talagrand (1991)). By applying the chain rule, we can aggregate these local Jacobians to obtain the complete derivative of the algorithm. This derivative takes the form of a product of Jacobian matrices. Notably, the associativity property of matrix multiplication empowers us to compute this matrix product in various orders.

Two prominent orders are particularly relevant: the forward order and the reverse order (see Fig.1). The forward order, also termed forward mode in the AD context, mimics the original algorithm's progression. In contrast, the reverse mode initiates its calculation from the Jacobian of the final elementary operation. The selection between these modes hinges on the characteristics of the function under consideration. In instances where the function is scalar, meaning it produces a solitary pertinent outcome (dependent variable) through mapping from multiple independent parameters, the reverse mode proves advantageous. This is the case when the problem evaluates a cost function. This preference arises because the reverse mode begins with a scalar sensitivity, which quantifies the derivative of the final result concerning itself (typically equal to one). Consequently, the reverse mode predominantly involves matrix-vector multiplications.

The forward mode corresponds to the tangent linear model (Fig.1 middle row), while the reverse mode corresponds to the adjoint model (Fig.1 bottom row). When confronted with scenarios featuring only a handful of independent parameters but yielding numerous dependent outcomes, the forward mode usually exhibits superior performance. This is when for instance one seeks to compute the gradient of the surface velocities of the convection model with respect to a limited set of material properties (viscosity parameters).

In the realm of AD, two primary methodologies have emerged. The first approach, known as AD by operator overloading (e.g. (Walther and Griewank (2012))), exploits a distinctive feature within programming languages. This feature allows the customization of individual operations, such as '*', to encompass additional computations for derivatives. In contrast, source-to-source AD tools adopt a different strategy. These tools, such as TAF (Giering and Kaminski (1998)) or TAPENADE (Hascoët and Pascual (2013)), generate novel derivative code within a specific programming language. This process mirrors the functioning of compilers, reading and parsing the existing code, analyzing its structure, and transforming its internal representation before reconstructing it (unparsing). The ensuing transformation adheres to either forward or reverse mode principles, yielding tangent linear or adjoint code correspondingly.

While the implemenation of AD by operator overloading as an automated tool is relatively easy compared to source-to-source AD, it comes at the expense of heightened resource demands in terms of memory and runtime for the resulting program. It is noteworthy that a multitude of AD tools now offer support for a range of different source code languages. The application of AD in geodynamics poses several challanges. These encompass the computational efficiency of the derivative code, compatibility with language standards of the source code, and accommodation for parallel computing like OpenMP, MPI, and coarray Fortran. Addressing these challenges is paramount to unlocking the full potential of Automatic Differentiation.

3.2 TAF: source-to-source translator

Transformation of Algorithms in Fortran (TAF) presents a valuable source-to-source AD tool, as detailed in (Giering and Kaminski (2002a)). TAF notably accommodates a wide spectrum of the Fortran standard, spanning from FORTRAN-77 through Fortran-2018. This versatility empowers TAF to generate both adjoint and tangent linear codes through reverse and forward modes, respectively.

The adjoint code excels in efficiently computing gradients, which find application in gradient-based optimization techniques. This is the case for geodynamic inversions, such as finding mantle convection initial conditions to generate an accurate prediction of a temperature structure interpreted from a tomographic model (Bunge et al. (2003); Liu et al. (2008)). Furthermore, this adjoint code can undergo differentiation once more. This subsequent differentiation generates code primed for the computation of the Hessian matrix. Within the realm of inversion problems, the inverse Hessian furnishes the uncertainty covariance matrix of the outcomes, thereby facilitating the proper utilization of the results in a meaningful manner.

The influence of source-to-source AD, demonstrated through TAF, resonates across a diverse spectrum of scientific domains. These domains include climatology (Blessing et al. (2014)), oceanography (Heimbach et al. (2005)), satellite remote sensing (Blessing and Giering (2021)), and engineering (Othmer et al. (2006)). Such versatility underscores the utility of TAF and analogous tools in addressing an array of complex problems that span multiple fields.

3.3 Taping and checkpointing

Given that the StagYY code, much like other advanced models in the geosciences domain, involves inherently solving nonlinear equations, the process of linearization is contingent on the prevailing system state (such as mantle temperature field in most cases). Consequently, for the propagation of sensitivities using reverse mode (i.e., the adjoint model), access to the system state becomes imperative. However, it is important to note that the adjoint model functions in reverse, navigating from the final state to the initial state. This contrasting operational directionality prompts a challenge: the states required for adjoint computations must be provided in the reverse order compared to their original computation sequence. In this context, two primary strategies exist: taping and recomputation.

Taping entails the storage of states either in memory or on external storage like disk. This stored data is then accessed when needed. On the other hand, an alternative approach involves recomputing a specific state based on an available initial or intermediate state (often referred to as a checkpoint). While the former demands additional memory or disk resources, the latter necessitates extra computational time. In practice, a judicious combination of both strategies, termed checkpointing, has demonstrated optimal outcomes. This approach minimizes the demand for substantial supplementary memory resources by introducing a modest increase in computational time (Griewank and Walther (2000); Giering and Kaminski (2002b)).

Within the StagYY framework, a pragmatic approach has been taken. TAF ”store”-directives have been integrated at the onset of the time-stepping loop and at various other strategic points. These directives effectively mitigate the need for default recomputations that arise from TAF, thus optimizing the sensitivity propagation process.

3.4 MPI

In the context of parallel computing in StagYY, the Message Passing Interface (MPI) plays a crucial role as the library of routines for enabling parallelism. It's important to note that, since MPI is not inherently integrated into the programming language, Automatic Differentiation (AD) tools must possess the capability to handle MPI library calls. This introduces a distinctive challenge that has given rise to three distinct approaches. One prevalent approach involves the implementation of MPI communication within separate, higher-level routines often referred to as 'wrapper' routines. These wrappers consolidate multiple individual communications for updating border grid points across neighboring domains in domain decomposition scenarios. The adjoint routines for these wrappers are manually crafted and AD-specific directives are inserted that provide the necessary information for the AD tool. This strategy has been successfully employed in parallelizing models like the global ocean-atmosphere circulation model MITgcm (Heimbach et al. (2005)). An alternative and more generalized approach has been proposed by (Utke et al. (2009)), extending frequently used MPI-library routines with additional arguments that carry essential information required for adjoint computation. Adjoint and tangent routines are then incorporated into an Adjoinable MPI (AMPI) library to enable the generation of proper calls to the modified MPI routines.

The third approach, employed in this context, entails the direct differentiation of MPI library calls by TAF. This methodology demands an additional global analysis of data transfer between processes, due to the low-level nature of MPI (one has to explicitly provide the details of the message passing). While collective communications, being group based and synchronized are relatively straightforward to implement, point-to-point (P2P) communications, especially non-blocking ones, pose a substantial challenge as they involve direct communication between two specific processes and involves asynchronicity. These non-blocking P2P communications consist of multiple MPI library calls, making their differentiation intricate. In the case of StagYY, which employs both collective and non-blocking P2P communications, the specific challenges of differentiating MPI library calls have been addressed. This intricate process is further detailed in an upcoming paper (Giering (2023)).

3.5 Changes to StagYY to apply TAF

Automatic Differentiation (AD) assumes a critical premise: that the algorithm under scrutiny behaves akin to a well-defined function, consistently producing the same outcomes for a given set of input values, which represent the control variables in our geodynamic problems. To make this work seamlessly, we have incorporated specialized interface routines. These routines serve as bridges between StagYY algorithms and the AD tool. They ensure that necessary initializations occur before an algorithm kicks into gear, they define the essential connections between inputs and outputs of the function, and they guarantee that the initial state is faithfully restored each time the function is invoked. Using pseudo-random numbers does not guarantee exact reproducibility between two runs. In this context, we switched them off to ensure the fidelity of these properties.

In order to help TAF to generate efficient adjoint code, directives have been inserted in STagYY in addition to the aforementioned "store"-directives which support the data flow analysis and ensure that the code generated by TAF is efficient and accurate.

4 RESULTS

4.1 Benchmarking preamble

In this section we present 2 cases of automatically generated 3D spherical convection adjoint codes and their benchmarking. The methodology to test the quality of adjoint codes is the gradient test (Navon et al. (1992); Andersson et al. (1994)), sometimes called Taylor test (Charpentier and Ghemires (2000)), an exacting benchmark for adjoint codes. It ensures the adjoint code is the exact adjoint of the forward code. Convergence of finite-difference towards the computed adjoint is not enough or not straightforward in the numerical context, because of the multiple factors which influence the computation of the finite-difference approximation. Obtaining the exact adjoint of the forward code, providing the exact numerical gradients is a key for an optimization process. Note that we do not perform optimization procedures to solve an inverse problem in the following work but we perform sensitivity evaluations.

We define a cost function $\mathcal{J}(\mathbf{x})$ for a state $\mathbf{x}$. The gradient test relies on a Taylor expansion of the cost function for a perturbed state $\mathbf{x} + \alpha\delta\mathbf{x}$:

$$\mathcal{J}(\mathbf{x} + \alpha\delta\mathbf{x}) = \mathcal{J}(\mathbf{x}) + \alpha\langle\nabla\mathcal{J}, \delta\mathbf{x}\rangle + \alpha^2\mathcal{O}(\delta\mathbf{x}^2), \tag{5}$$

where α is a scalar defining the intensity of the perturbation, $\delta\mathbf{x}$ a random perturbation vector comensurate with $\mathbf{x}$ and $\langle\nabla\mathcal{J},\delta\mathbf{x}\rangle$ the sensitivity of $\mathcal{J}$ to a perturbation in $\mathbf{x}$. The latter is given by running the adjoint code while $\mathcal{J}(\mathbf{x})$ and $\mathcal{J}(\mathbf{x}+\alpha\delta\mathbf{x})$ are computed with the forward code. The residue being

$$\mathcal{R}(\alpha) = \mathcal{J}(\mathbf{x}+\alpha\delta\mathbf{x}) - \mathcal{J}(\mathbf{x}) - \alpha\langle\nabla\mathcal{J},\delta\mathbf{x}\rangle \tag{6}$$

has therefore to scale with α^2. This test does multiple things at once. It helps to identify the range for which the truncated Taylor expansion is a good approximation to the gradient ($\mathcal{R}(\alpha)\sim\alpha^2$ range), the range where the finite-differences approximation is the numerically best-possible approximation to the gradient ($\mathcal{R}(\alpha)\sim const.$ range), and the range where α is too small to make a difference numerically in $\mathcal{J}(\mathbf{x}+\alpha\delta\mathbf{x})$ ($\mathcal{R}(\alpha)\sim\alpha$ range). If these ranges can be identified, there is confidence that the finite-differences-approximation of the gradient would converge to the gradient computed with the adjoint if there were no limitations in numerical representation.

4.2 A benchmarking example

We generate automatically an adjoint code to illustrate and benchmark the workflow. The goal of the following test is to explore specific capabilities that could be used for mantle convection inverse problems, but using a simplified abstract case, which targets the computation of the sensitivities of an initial temperature field to the error between a predicted state and a known temperature field. The corresponding adjoint code would be relevant to the published strategies for inferring past mantle circulation (Bunge et al. (2003); Ismail-Zadeh et al. (2003); Ismail-Zadeh et al. (2004); Liu and Gurnis (2008)). The test we implement focuses mainly on transport of heat and composition. The code uses the multi-grid solver of StagYY, the yin-yang-layout of the grid and the tracer ratio method.

In the adjoint code, the specific heat field is the control variable, being in this case the local temperature times the cell volume (the problem hereafter being incompressible and in its non-dimensional form). The cost function evaluates the heat difference between the predicted state and the reference state:

$$\mathcal{J}^T = \sum_i^{\mathcal{V}} \left(T(x_i) - T_0(x_i)\right)^2 \Delta V(x_i), \tag{7}$$

where T is the final volume-centered temperature in the model, T_0 the targeted final volume-centered temperature field, (x_i) the coordinates of the cell center and ΔV the value of the local volume (the global volume being V). The summation is over full volume $\mathcal{V}$. Such adjoint code could in principle be used to retrieve the initial conditions to match a final temperature structure deduced from seismic tomography (Bunge et al. (2003); Ismail-Zadeh et al. (2003); Ismail-Zadeh et al. (2004); Liu et al. (2008)). This adjoint code generated by TAF is 270 399 lines while the forward code is 75 960 lines.

Parameter	Non dimensional value
Rayleigh number	10^6
Heat production rate	35
Top temperature	0
Basal temperature	1
Depth of basal layer	0.3
Viscosity of basal layer	50
Buoyancy ratio of basal layer	1
Number of cells	786 432
Number of tracers	8 000 000
Average resolution	90 km

Table 1. Non dimensional parameters of the convection model used for benchmarking the adjoint code

A fraction of the increased number of lines comes from the fact that the adjoint code has one line for one variable declaration whereas the forward code can have one line of several variable declarations.

We perform a gradient test to verify the adjoint code is the exact adjoint of the forward code. For this benchmarking case, we specifically choose an abstract case for 2 goals: being easily computed so it has to be small enough; using a variety of the code capabilities so it has to be complex enough. The rheological complexity is explored in the following geodynamic application. We choose an incompressible 3D spherical convection model with a composition-dependent viscosity, the goal being here to focus on the time-dependent transport sections of the code (temperature and composition). We consider two materials here: ambient mantle and a deep dense and more viscous layer. The properties of this layer are set to typical values suitable to study the stability of a primordial dense viscous layer on a planet (such as in (Kreielkamp et al., (2002))). We solve the composition evolution equation using the tracer ratio method. The set of parameters for the model is in Table 1. The forward calculation corresponds to the convection evolution from a designed initial condition and runs over 10 time steps equivalent to a dimensionless time of 10^{-5} (equivalent of 3 My), being enough to start develop the instabilities (see Fig.2). More timesteps would require to implement specific strategies for taping to optimize computing speed, which is not the goal here. Fig.2 shows the initial and final temperature and compositions fields for the trial and the targeted temperature field.

The sensitivity obtained running the adjoint code is shown in Fig. 3. In the volume section, we identify that heating the initial state would decrease the cost function and we can identify areas in upwellings that should be cooled off. For the gradient test, we compute $\mathcal{R}(\alpha)$ for a variety of α between 10^{-15} to 10^{-4}, using a vector $\delta\mathbf{x}$, which individual components are random numbers ranging from 0 to 1. The cost function for this case is 3.561. $\mathcal{R}(\alpha)$ reaches the machine ε for $alpha$ around 10^{-12}. $\mathcal{R}(\alpha)$ decreases as α^2 for larger values of α and becomes more linear as the machine ε is reached.

Without optimization, this automatically generated adjoint code passes the gradient test. This adjoint runs 11 times slower than the forward code, the latter running in 39 seconds over 32 cores on an AMD Ryzen Threadripper 3990X processor.

4.3 Sensitivity of surface kinematics to convective mantle temperature structure

4.3.1 Forward problem

We now automatically generate an adjoint code to estimate the sensitivity of surface velocities to temperature anomalies in the mantle-lithosphere system. We consider here a 3D spherical convection model with plate-like behavior, which we will use for instantaneous calculation of mantle flow and surface kinematics. Viscosity depends exponentially on temperature and depth:

$$\mu(z,T) = \mu_0(z) \exp \frac{E_a}{T}$$

with μ being the dimensionless viscosity, $\mu_0(z)$ the viscosity prefactor, Ea the activitation energy, and T the absolute dimensionless temperature.

$\mu_0(z)$ is chosen (1) to obtain a reference dimensionless viscosity is 1 for a non-dimensional temperature of 0.64 at zero pressure, the expected temperature at the base of the cold boundary layer before the realization of the calculation, and (2) to allow for a viscosity jump at 660 km as expected from geoid inversions(Ricard et al. (1993)), although this depth could be extended deeper (Rudolph et al. (2015)). This specific value is selected prior to the calculation to align with the anticipated temperature at the base of the upper boundary layer. To prevent excessive variations in viscosity, a maximum non-dimensional viscosity of 10^4 is enforced as a cutoff. Consequently, before performing the calculation, it is expected that there will be a viscosity contrast of 10^4 across the upper boundary layer. Following the calculation, the average non-dimensional temperature at the base of the upper boundary layer is determined to be 0.75, indicating that it is somewhat hotter than initially anticipated. However, it remains stable. Consequently, as illustrated in Figure 2, the typical non-dimensional viscosity in the upper mantle, excluding the slabs is around 10^{-1}.

The viscosity is also stress dependent, as we include a yield stress formulation so high strain rates can localize in the boundary layer to generate analogs of plate-boundaries (Coltice et al. (2017)). The yield stress depends weakly on depth here. The parameters used for the convection model are presented in Table 2 and are set to generate plate-like behavior at statistical steady-state.

We will use here two guesses for the temperature field. We will use a constant temperature in order

Parameter	Non dimensional value
Rayleigh number	10^6
Heat production rate	35
Top temperature	0.12
Basal temperature	1.12
Temperature for the viscosity of reference (1)	0.64
Viscosity jump factor at depth 0.227 (660 km)	30
Activation energy	8
Yield stress at the surface	10^4
Yield stress depth derivative	0.025
Number of cells	6 258 688
Average resolution	45 km

Table 2. Non dimensional parameters of the convection model used predicting Earth surface velocities

to evaluate the sensitivity of a model without any information (here we use a temperature guess of 0.7 similar to the average temperature obtained in the following model). We will also use a temperature field build by imposing the plate motion model of (Seton et al. (2012)) over a convection model. This setup, called hereafter 'nudged', is very similar to (Coltice and Shephard (2018)). Therefore, we refer to this paper for more details on the modelling of the temperature field.

Predicting global kinematics by computing whole mantle flow has been a challenge since more than 40 years ago (Hager and O'Connell (1979)). (Ricard and Vigny (1989)), (Becker and O'Connell (2001)) or (Conrad and Lithgow-Bertelloni (2002)) achieved accurate plate motion predictions, albeit with slightly different guessed density models within the Earth's mantle, using radially a constant viscosity structure and prescribing a priori plate geometry and rigidity. (Stadler et al. (2010)), (Alisic et al. (2012)) and (Ghosh and Holt (2012)) accurately predicted plate motions based on a guessed temperature field derived from seismology, considering lateral viscosity variations, internal deformation of plates and variable strength of plate boundaries. Our model differs from these studies two noteworthy manners: (1) we allow rigid plates or plate boundaries to emerge self-consistently from local force balance while these studies impose the plate layout a priori; and (2) our model treats these temperature fields as outputs given by running the "nudged" convection model, meaning that there is a degree of self-consistency between the density structure and the self-organized state of the system, while the previously mentioned studies use guesses of the density structure by converting seismic anomalies or imposing the location of slabs in the mantle.

We derive below the sensitivity structure of plate kinematics to the 3D temperature field, which contributes to the flow through both buoyancy anomalies and viscosity contrasts.

4.3.2 Adjoint code and gradient test

The full temperature field is the control variable, as in the first adjoint code. The cost function of the second code is

$$\mathcal{J}^{\mathbf{v}} = \frac{1}{S}\sum_{i}^{\mathcal{S}} \langle \mathbf{v}(x_i) - \mathbf{v}_0(x_i), \mathbf{v}(x_i) - \mathbf{v}_0(x_i)\rangle \Delta S(x_i), \tag{8}$$

where $\mathbf{v}(x_i)$ is the velocity at the volume center, $\mathbf{v}_0(x_i)$ the target velocity at the volume center. The summation is over the surface of the model $\mathcal{S}$, $\Delta S(x_i)$ being the local elemental surface. The generated adjoint code gives the sensitivity to the initial temperature field of the full flow difference with respect to the plate kinematic model of (Seton et al. (2012)) for consistency. Since there is no covariance weighting in the cost function, the misfit being of the order of magnitude of the velocity itself, high velocities can dominate the misfit here. This adjoint code generated by TAF is 270 034 lines. Since the control variable is the same as in the benchmarking case, the core of this generated adjoint code is very similar to that of the benchmarking example.

4.3.3 Sensitivity of uniform temperature structure

We first set a uniform temperature structure. As a consequence, the predicted surface velocities are only null vectors, the cost function representing then the mean squared surface velocity. The uniform thermal state implies there is not cold boundary layer where yielding can occur. Running the adjoint code on that setup offers a way to evaluate the location of temperature anomalies that contribute to generate the expected kinematics. However, given the non-linear relationship between temperature and velocity in the present model, it should not be mistaken as the kernels used in (Forte and Peltier (1991)) or (Vigny et al. (1991)).

The sensitivity fields depicted in Fig. 7 show the upper mantle dominates the signal over the lower mantle by more than an order of magnitude in the presence of the viscosity jump at 660 km. At this depth, the average sensitivity changes sign. Hence, in the upper mantle negative temperature anomalies would reduce the cost function, while in the lower mantle positive anomalies would be required. This prediction is consistent with slabs in the upper mantle being the essentials in driving plate motions (Conrad and Lithgow-Bertelloni (2002); Coltice et al. (2019)). The sensitivity structure observed in the cross section (right column of Fig. 7) suggests creating temperature contrasts in the upper mantle across plate boundary locations would be favorable to decrease the cost function. Such temperature distribution does not corresponds to typical convection planform. It shows further interpretation should be done with the awareness that the adjoint is a linear estimate of the sensitivity around the guessed state (Talagrand (1997)). We see here that such a distant guess from the awaited solution combined with a non-linear rheology is not appropriate for starting an inversion process.

Increasing the yield stress by a factor of 2 has the effect of decreasing the sensitivities while keeping the structure similar (second row of Fig. 7). This means that temperature anomalies should be stronger to impact more the flow than with a smaller yield stress. It is consistent with the fact that stronger buoyancy forces are required to generate larger stresses so that yielding is reached to generate plate boundaries and surface mobility. The average sensitivities as a function of depth has a similar behavior as the lower yield stress case.

The rms of the adjoint field (first column, third row in Fig. 7) shows that the removing the viscosity jump at 660 km smoothes out sensitivity contrast between upper and lower mantle. Deeper thermal anomalies impact surface velocities. The magnitude of the sensitivity is smaller by more than 3 orders of magnitude than with a viscosity jump, meaning that the cost function is less sensitive to a local given temperature anomaly than in the model with a viscosity jump. This is consistent with the fact that the sensitivity without a viscosity jump is more distributed within the whole mantle. The changes of sign of the average sensitivity with depth suggests that reducing the cost function would be favored by hotter anomalies in the shallow and lower mantle, while cold anomalies around 500 km. Although these differences with the layered viscosity case, the cross section in Fig. 7 shows that the structure of the adjoint field remains similar.

4.3.4 Sensitivity of nudged temperature structure

We compute the sensitivity of the nudged temperature structure. We use a forward model run to compute the full 3D velocity field in response to the ”nudged” temperature field. No plate structure or velocities are imposed here. Both plate boundary positions and kinematics are predictions of the forward model. The comparison between this prediction and the velocities from the plate reconstructions show the mismatch between the model and the observations. The sensitivities obtained by running the adjoint code estimate the correction to improve the prediction. Fig. 8 shows that the forward run represents consistently the main ridge and trench systems but fails in expressing the African rift and the smaller scale connection between convergent plate boundaries in the East Pacific system. Velocities are consistent in direction and magnitude in major areas of the world (Atlantic, Indian and Pacific ocean). However, the Pacific plate is slower than expected and the convergence directions across South America is deviated towards the South compared to what is expected. Unlike the previous uniform state, this one closely aligns with the expected state, as it accurately reproduces the key characteristics of plate motions. As a reminder for the reader, plate boundaries in this model emerge self-consistently in the numerical solution and are not prescribed by the modeler through weaker areas.

The sensitivity structure is shown in Fig.9 for the reference model (top row) and for a model in which the yield stress value is twice the reference (bottom row). Both adjoint rms sensitivity profiles show 3 peaks in sensitivity: in the lithosphere, in the mid-mantle and at the bottom of the mantle. Areas where the model is the most sensitive represent a combination of errors in the temperature structure and intrinsic sensitivity of the surface velocities to these areas (surface velocities are in principle less sensitive to the deeper mantle as shown in the previous subsection).

The computed sensitivity show that small temperature changes in the lithosphere have a strong impact on the cost function. Because forces in the lithosphere dominate the force balance (slab pull corresponds to pressure gradients within the lithosphere), it is expected that small alteration of this balance modify the surface flow. From the significantly higher RMS sensitivity compared to the average, we anticipate that for a plate, heating up a ridge and cooling down a trench could yield comparable effects.

While previous uniform guessed states predict a low sensitivity to lower mantle thermal structure, the nudged guesses show a comparable sensitivity of the upper and lower mantle structure. Our interpretation lies in the way the nudged temperature field is built: plate kinematics is more precise for recent times, and consequently, we expect the upper mantle structure to be represented with greater consistency than the deeper mantle. Therefore the deep mantle thermal structure is probably the less consistent with the surface flow, which would need the more correction for a better fit. An area in which the structure is consistent with the prediction would have a low sensitivity, while an area in which the structure is not consistent would have a high sensitivity. It is then expected that the deeper mantle is a place of high sensitivity. The mid-mantle is the area where slabs that enter the more viscous lower mantle tend to flatten and fold. Therefore this area generates major structures for the global organization of the flow. The viscosity change which impacts the most the flow in this area is the subject of debates (Rudolph et al. (2015)) and therefore small errors on its parameterization could result in generating erroneous deep slab structures. The change of sign of the average sensitivity in the reference model shows that reducing the cost function would require heating up the base of the mantle while increasing the amount of cold anomalies between 1000 and 2000 km. Fig.9 which matches cross section in Fig.5) reveals that the thermal structure beneath plate boundaries and in the environment of slabs dominate the sensitivity signal. The same figure shows that surface velocities are not very sensitive to plume structures.

Increasing the yield stress in the model shows a similar overall structure but specific differences. First of all, and consistently with the uniform structure cases, the sensitivity is lower. Stronger temperature anomalies would be required to lower the cost function compared to the reference model. The high yield stress model is more sensitive to cold temperature changes in the top boundary layer. The signal is now more confined in the top and bottom regions of the model, for the same reasons as advocated in the previous paragraph. Contrarily to the reference model, with a high yield stress cooling the deeper mantle and heating up the 1000 km-2000 km area are predicted to decrease the cost function. It suggests that resolving these areas in mantle reconstructions can be strongly dependent on the given rheological structure.

5 DISCUSSION AND CONCLUSIONS

We have presented here the development of the automatic generation of adjoint codes for the sophisticated parallel multi-geometry thermochemical convection code StagYY. As opposed to inversions which require combining forward and adjoint calculations embeded into an optimization scheme, we have focused on the direct output of adjoint codes: sensitivities with a specific application to how surface velocities are sensitive to the 3D thermal structure of the mantle. The generation of adjoint codes relies on implementing point to point MPI automatic differentiation in TAF, and the adaptation of StagYY code being mostly inserting TAF directives. We have created this workflow to make sure the adjoint code is the exact adjoint of the forward code. Solving adjoint equations does not give such guarantee. The gradient test, also called Taylor test, is the exacting validation test for such property, which is fundamental to make sure adjoint codes give the best estimates in a minimization/inversion process. A finite difference check of the adjoint is not enough to benchmark an adjoint code. The specific dependence of the finite-difference convergence needs to be evaluated.

Another reason to use automatic differentiation is that changing the control variable (or cost function but in a very moderate manner) requires the development of a new adjoint code: one sensitivity problem needs one specific adjoint code. To finish with, StagYY has 20 years of evolution and will evolve. New physics, new solvers, new methods will be added to it (grain size dynamics, melting,...) implying following changes in adjoint codes. Maintaining the code structure which is prerequisite for differentiation, we can generate new adjoint codes automatically. Since we expect a multitude of inverse problem for mantle convection/plate tectonics modelling, the automatic differentiation approach remains versatile, sustainable and efficient.

We have presented here a benchmarking test focused on generating an adjoint code that can be used to recover initial conditions knowing a final temperature distribution, which has been proposed as an inverse problem for mantle convection, using tomographic models as thermal proxies. We have used tracers to track the composition in such models introducing a coupling between composition and momentum equations.

We then generated an adjoint code to compute the sensitivity of surface velocities to the internal 3D thermal structure of a mantle convection calculation with plate-like behavior, introducing complexities in system equations and numerical methods. After performing a gradient test, we have computed model sensitivities with two different temperature structure: uniform and nudged with a plate kinematic model. The uniform temperature distribution show that the presence of a viscosity jump at 660 km make the surface velocities poorly sensitive to lower mantle temperature anomalies, while the value of the yield stress impacts the magnitude of the sensitivity (low yield stress means high sensitivity). The nudged temperature structure suggest that lower mantle structure predictions are difficult to realize because of uncertainties in the rheological parameterization and in plate kinematic models before 50 My. The upper boundary layer expresses the stronger sensitivities, consistently with the dominance of forces like slab pull, ridge push, and lithospheric/crustal thickness anomalies, all of them generating pressure gradients in the boundary layer.

The generation of adjoint codes is a first step towards solving optimisation problems and therefore to embed models together with observations. For a given problem, the adjoint code which is automatically generated can require some optimisation, mostly on memory use and choices of checkpointing and recomputation. Also the development of an optimisation procedure that can handle the fact that mantle convection problems can be non-linear and non-Gaussian, especially when using non-linear rheologies, is a step to make. Another difficulty is the size of such problems with non-linear rheologies and high resolution in 3D. Adjoints created with TAF typically require a computational time of about 2 to 5 times of that of the forward code, where the adjoint run includes the computation of the cost function, which is necessary for non-linear problems and we hope to overcome the worse performance of the presented codes in the near future. But still, together with the model approximations (rheology, compressibility) and sparsity of data (no direct observation of Earth's interior), computing time will be the most limiting factors towards global geodynamic inversions.

ACKNOWLEDGMENTS

DATA AVAILABILITY

The data used for running the test and making the figures are available in the following repository: https://osf.io/dpzv8/

The convection code StagYY is the property of P.J.T. and EidgeniÃ¶ssische Technische Hochschule (ETH) ZÃŒrich. Researchers interested in using StagYY should contact P.J.T. (paul.tackley@erdw.ethz.ch), and N.C. (nicolas.coltice@ens.fr) for the TAF compliant version of StagYY.

The adjoint code was generated with TAF. A TAF license is available from FastOpt.

REFERENCES

Alisic, L., Gurnis, M., Stadler, G., Burstedde, C., and Ghattas, O., (2012). Multiscale dynamics and rheology of mantle flow with plates. *J. Geophys. Res.*, **117**, B10402.

Andersson, E., Pailleux, J., Thépaut, J.-N., Eyre, J.R., McNally, A.P., Kelly, G.A. and Courtier, P., 1994. Use of cloud-cleared radiances in three/four-dimensional variational data assimilation. *Quarterly J. of the Roy. Meteo. Soc.*, **120**, 627–653.

Armann, M. and Tackley, P.J., 2012. Simulating the thermo-chemical magmatic and tectonic evolution of Venus' mantle and lithosphere: two-dimensional models. *J. Geophys. Res.*, **117**, E12003, doi:10.1029/2012JE004231.

Arnould, M., Coltice, N. and Flament, N. and Mallard, C., 2020. Plate tectonics and mantle controls on plume dynamics. *Earth and Planet. Sci. Lett.*, **547**, 116439.

Baumann, T.S., Kaus, B.J.P. and Popov, A., 2014. Constraining effective rheology through parallel joint geodynamic inversion. *Tectonophys.*, **631**, 197–211.

Becker, T. W., and O'Connell, R. J., (2001). Predicting plate velocities with mantle circulation models. *Geochem. Geophys. Geosys.*, **2**, 12.

Bello, L., Coltice, N., Tackley, P.J., Dietmar MÃŒller, R. and Cannon, J., 2015. Assessing the role of slab rheology in coupled plate-mantle convection models. *Earth Planet. Sci. Lett.*, **430**, 191–201.

Blessing, S. and Giering, R., 2021. Simultaneous retrieval of soil, leaf, and canopy parameters from sentinel-3 OLCI and SLSTR multi-spectral top-of-canopy reflectances, *preprint*.(doi: 10.20944/preprints202109.0147.v1)

Blessing, S., Kaminski, T., Lunkeit, F., Matei, I., Giering, R., Koehl, A., Scholze, M., Herrmann, P., Fraedrich, K., and Stammer, D., 2014. Testing variational estimation of process parameters and initial conditions of an earth system model, *Tellus, Series A: Dynamic Meteorology and Oceanography*, **66**.

Bocher, M., Coltice, N. and Fournier, A. and Tackley, PJ., 2016. A sequential data assimilation approach for the joint reconstruction of mantle convection and surface tectonics. *Geophys. J. Int.*, **204**, 200–214.

Bocher, M., Fournier, A. and Coltice, N. , 2018. Ensemble Kalman filter for the reconstruction of the Earth's mantle circulation. *Nonlin. Processes in Geophys.*, **25**, 99–123.

Borgeat, X. and Tackley, P.J., 2022. Hadean/Eoarchean tectonics and mantle mixing induced by impacts: a three-dimensional study. *Progress Earth Planet. Sci.*, **9**, DOI:10.1186/s40645-022-00497-0.

Bunge, H.-P., Richards, M. A. and Baumgardner, J. R., 1996. Effect of depth-dependent viscosity on the planform of mantle convection. *Nature*, **379**, 436–438.

Bunge, H.-P. and Grand, S.P., 2000. Mesozoic plate-motion history below the northeast Pacific Ocean from seismic images of the subducted Farallon slab. *Nature*, **405**, 337–340.

Bunge, H.-P. and Hagelberg, C. R. and Travis, B. J., 2003. Mantle circulation models with variational data assimilation: inferring past mantle flow and structure from plate motion histories and seismic tomography. *Geophys. J. Int.*, **152**, 280–301.

Charpentier, I. and Ghemires, M., 2000. Efficient adjoint derivatives: application to the meteorological model

Meso-NH. *Optimization Methods and Software*, **13**, 35–63.

Colli, L., Ghelichkhan, S., Bunge, H. P., and Oeser, J., 2018. Retrodictions of Mid Paleogene mantle flow and dynamic topography in the Atlantic region from compressible high resolution adjoint mantle convection models: Sensitivity to deep mantle viscosity and tomographic input model. *Gondwana Res.*, **53**, 252–272.

Coltice N., Rolf T. and P. J. Tackley and Labrosse S., 2012. Dynamic Causes of the Relation Between Area and Age of the Ocean Floor. *Science*, **336**, 335–338.

Coltice, N., Gérault, Mélanie and Ulvrová, Martina, 2017. A mantle convection perspective on global tectonics. *Earth-Sci. Rev.*, **165**, 120–150.

Coltice, N. and Shephard, Grace E., 2018. Tectonic predictions with mantle convection models. *Geophys. J. Int.*, **213**, 16–29.

Coltice, N., Husson, L., Faccenna, C. and Arnould, M., 2019. What drives tectonic plates? *Sci. advances*, **5**, eaax4295.

Conrad, C. P., and Lithgow-Bertelloni, C., (2002). How mantle slabs drive plate tectonics. *Science*, **298**, 207–209.

Crameri, F., Schmeling, H., Golabek, G.J., Duretz, T., Orendt, R., Buiter, S.J.H., May, D.A., Kaus, B.J.P., Gerya, T.V. and Tackley P.J., 2011. A comparison of numerical surface topography calculations in geodynamic modelling: an evaluation of the sticky air method. *Geophys. J. Int.*, **189**, 3854

Crameri, F. and Tackley, P.J., 2014. Spontaneous development of arcuate single-sided subduction in global 3-D mantle convection models with a free surface. *J. Geophys. Res.*, **119**, 5921–5942.

Ghosh, A., and Holt, W. E., (2012). Plate motions and stresses from global dynamic models. *Science*, **335**, 838–843.

Hager, B. H., and O'Connell, R. J. (1979). Kinematic models of large scale flow in the Earth's mantle. *J. Geophys. Res.*, **84**, 1031–1048.

Forte, A. M. and Peltier, R., 1991 Viscous flow models of global geophysical observables: 1. Forward problems. *J. Geophys. Res.*, **96**, 20131–20159.

Ghelichkhan, S. and Bunge, H. P., 2018. The adjoint equations for thermochemical compressible mantle convection: derivation and verification by twin experiments. *Proc. of the Roy. Soc. A*, **43**, 2510–2516.

Giering, R. and Kaminski, T., 2003. Applying TAF to generate efficient derivative code of Fortran 77 & 95 programs. *Proc. in Applied Math. and Mech.*, **2**, 54–57.

Giering, R., 2023. Direct differentiation of MPI library calls, submitted to *ACM Transactions on Mathematical Software*.

Giering, R. and Kaminski, T., 1998. Recipes for adjoint code construction, *ACM Transactions on Mathematical Software*, **24**(4), 437–474.

Giering, R. and Kaminski, T., 2002a. Applying TAF to generate efficient derivative code of Fortran 77-95 programs. In *Proceedings of GAMM 2002, Augsburg, Germany*.

Giering, R. and Kaminski, T., 2002b. Recomputations in reverse mode AD. In *Automatic Differentiation: From Simulation to Optimization*, Computer and Information Science, chap. 33, pp. 283–291, eds. Corliss, G., Faure, C., Griewank, A., Hascoët, L., and Naumann, U., Springer, New York.

Giering, R., T. Kaminski, and T. Slawig, 2005. Generating efficient derivative code with TAF: Adjoint and tangent linear Euler flow around an airfoil. *Future Generation Computer Systems*, **21**(8), 1345–1355, DOI: 10.1016/j.future.2004.11.003.

Grand, S. P. and van der Hilst, R. D. and Widiyantoro, S., 1997. Global seismic tomography; a snapshot of convection in the Earth. *GSA Today*, **7**, 1–7.

Griewank, A. and Walther, A., 2000. Algorithm 799: Revolve: An implementation of checkpoint for the reverse or adjoint mode of computational differentiation, *ACM Transactions on Mathematical Software*, **26**(1), 19–45, Also appeared as Technical University of Dresden, Technical Report IOKOMO-04-1997.

Hascoët, L. and Pascual, V., 2013. The Tapenade Automatic Differentiation tool: Principles, Model, and Specification, *ACM Transactions On Mathematical Software*, **39**(3).

P. Heimbach and C. Hill and R. Giering, 2005. An efficient exact adjoint of the parallel MIT general circulation model, generated via automatic differentiation, *Future Generation Computer Systems*, **21**(8), 1356–1371.

Hernlund, J. W. and Tackley P.J., 2008. Modeling mantle convection in the spherical annulus. *Phys. Earth and Planet. Int.*, **171**, 48–54.

Ismail-Zadeh, A.T., Korotkii, A.I., Naimark, B.M., and Tsepelev, I.A., (2003). Three-dimensional numerical simulation of the inverse problem of thermal convection. *Comp. Math. Math. Phys.*, **43**, 581–599.

Ismail-Zadeh, A., Schubert, G., Tsepelev, I., and Korotkii, A., (2004). Inverse problem of thermal convection: numerical approach and application to mantle plume restoration. *Phys. Earth Planet. Int.*, **145**, 99–114.

Jain, C., Rozel, A. B., Tackley, P. J., Sanan, P. and T. V. Gerya, 2019. Growing primordial continental crust self-consistently in global mantle convection models. *Gondwana Res.*, **73**, 96–122.

Kageyama, A. and Sato, T., 2004. The "Yin-Yang grid": An overset grid in spherical geometry. *Geochem. Geophys. Geosyst.*, **5**, doi:10.1029/2004GC000734.

Keller, T. and Tackley P.J., 2009. Towards self-consistent modelling of the Martian dichotomy: The influence of low-degree convection on crustal thickness distribution. *Icarus.*, **202**, 429–443.

Kreielkamp, P., Stein, C. and Hansen, U., 2002. LLSVPs of primordial origin: Implications for the evolution of plate tectonics. *Earth Planet. Sci. Lett.*, **579**, 117357.

Langemeyer, S.M., Lowman, J.P. and Tackley, P.J., 2021. Global mantle convection models produce transform offsets along divergent plate boundaries. *Comm. Earth & Environment*, **1**, 1–10.

Li, D., Gurnis, M. and Stadler, G., 2017. Towards adjoint-based inversion of time-dependent mantle convection with nonlinear viscosity. *Geophys. J. Int.*, **209**, 86–105.

Liu, L. and Gurnis, M., 2008 Simultaneous inversion of mantle properties and initial conditions using an adjoint of mantle convection. *J. of Geophy. Res.: Solid Earth*, **113**, B8.

Liu, L. and Spasojevic, S. and Gurnis, M., 2008 Reconstructing Farallon plate subduction beneath North America back to the Late Cretaceous. *Science*, **322**, 934–938.

Mallard, C., Coltice, N., Seton, M., Müller, R.D. and Tackley, P.J., 2016. Subduction controls the distribution and fragmentation of Earth's tectonic plates. *Nature*, **535**, 140–143.

Martin, N., and Monnier, J., 2014. Adjoint accuracy for the full Stokes ice flow model: limits to the transmission of basal friction variability to the surface. *The Cryosphere*, **8**, 721–741.

Navon, I. M., Zou, X., Derber, J. and Sela, J., 1992. Variational data assimilation with an adiabatic version of the NMC spectral model. *Monthly Weather Rev.*, **120**, 1433–1446.

Nakagawa, T., Tackley, P.J., 2004. Effects of thermo-chemical mantle convection on the thermal evolution of the Earth's core. *Earth Planet. Sci. Lett.*, **220**, 107–119.

Ogawa, M., Schubert, G., and Zebib, A., 1991. Numerical simulations of 3-dimensional thermal convection in a fluid with strongly temperature-dependent viscosity *J. Fluid Mech.*, **233**, 299-328.

Othmer, C., Kaminski, T., and Giering, R., 2006. Computation of topological sensitivities in fluid dynamics: Cost function versatility. In *ECCOMAS CFD 2006*, TU Delft.

Patankar, S. V., 1980. Numerical Heat Transfer and Fluid Flow. *Hemisphere Publishing Corporation, New York*.

Patočka, V., Čadek O, Tackley, P. J. and Čižková, H., 2017. Stress memory effect in viscoelastic stagnant lid convection *Geophys. J. Int.*, **209**, 1462–1475.

Ratnaswamy, V. and Stadler, G. and Gurnis, M., 2015. Adjoint-based estimation of plate coupling in a non-linear mantle flow model: theory and examples. *Geophys. J. Int.*, **202**, 768–786.

Reuber, G. S., Holbach, L., Popov, A. A., Hanke, M. and Kaus, B. J., 2020. Inferring rheology and geometry of subsurface structures by adjoint-based inversion of principal stress directions. *Geophys. J. Int.*, **223**, 851–861.

Ricard, Y., and Vigny, C., (1989). Mantle dynamics with induced plate tectonics. *J. Geophys. Res.*, **94**, 17543–17559.

Ricard, Y., Richards, M., Lithgow-Bertelloni, C., and Le Stunff, Y., (1993). A geodynamic model of mantle density heterogeneity. *J. Geophys. Res.*, **98**, 21895–21909.

Ricard, Y., Alboussière, T., Labrosse, S., Curbelo, J. and Dubuffet, F. (2022). Fully compressible convection for planetary mantles. *Geophys. J. Int.*, **230**, 932–956.

Rolf, T., Coltice, N. and Tackley, P.J., 2014. Statistical cyclicity of the supercontinent cycle. *Geophys. Res. Lett.*, **41**, 2351–2358.

Rudolph, M. L., Lekic, V., and Lithgow-Bertelloni, C., (2015). Viscosity jump in Earth's mid-mantle. *Science*, **350**, 1349–1352.

Seton, M., Müller R.D., Zahirovic, S., Gaina, C., Torsvik, T., Shephard, G ., Talsma, A., Gurnis, M., Turner, M. and Maus, S., (2012). Global continental and ocean basin reconstructions since 200 Ma. *Earth Sci. Rev.*, **113**, 212–270.

Stadler, G., Gurnis, M., Burstedde, C., Wilcox, L. C., Alisic, L., and Ghattas, O., (2010). The dynamics of plate tectonics and mantle flow: From local to global scales. *Science*, **329**, 1033–1038.

Tackley, P. J., 2000. Mantle convection and plate tectonics: Toward an integrated physical and chemical theory *Science*, **288**, 2002-2007.

Tackley, P. J., 1993. Effects of strongly temperature-dependent viscosity on time-dependent, 3-dimensional models of mantle convection *Geophys. Res. Lett.*, **20**, 2187–2190.

Tackley, P. J., 1996. Effects of strongly variable viscosity on three-dimensional compressible convection in planetary mantles *J. Geophys. Res.*, **101**, 3311–3332.

Tackley, P. J., 1998. Self-consistent generation of tectonic plates in three-dimensional mantle convection *Earth Planet. Sci Lett.*, **157**, 9–22.

Tackley, P. J., 1998. Three-dimensional simulations of mantle convection with a thermochemical CMB boundary layer: D"? *M. Gurnis, M.E. Wysession, E. Knittle and B.A. Buffett (eds.), The Core-Mantle Boundary Region (American Geophysical Union)*, **28**, 231–253.

Tackley, P. J., 2000. Self-consistent generation of tectonic plates in time-dependent, three-dimensional mantle convection simulations 1. Pseudoplastic yielding *Geochem. Geophys. Geosys.*, **1**, 2000GC000036.

Tackley, P. J., 2001. Convection in Io's asthenosphere: Redistribution of non-uniform tidal heating by mean flows *J. Geophys. Res.*, **106**, 32971–32981.

Tackley, P. J. and King, S. D., 2003. Testing the tracer ratio method for modeling active compositional fields in mantle convection simulations *Geochem, Geophys. Geosyst.*, **4**, doi:10.1029/2001GC000214.

Tackley P.J., 2017. Modelling compressible mantle convection with large viscosity contrasts in a three-dimensional spherical shell using the yin-yang grid. *Phys. Earth and Planet. Int.*, **71**, 7–18.

Tackley, P.J., 2012. Dynamics and evolution of the deep mantle resulting from thermal, chemical, phase and melting effects. *Earth-Sci. Rev.*, **110**, 1–25.

Tackley, P.J., Ammann, M., Brodholt J. P., Dobson, D. P. and Valencia, D., 2012. Mantle dynamics in super-Earths: Post-perovskite rheology and self-regulation of viscosity. *Icarus*, **110**, 50–61.

Talagrand, O., 1991. The use of adjoint equations in numerical modelling of the atmospheric circulation. In *In Automatic differentiation of algorithms: theory, implementation, and application*, A. Griewank and G. Corliess Eds., pp. 169-180. Philadelphia, Penn: SIAM.

Talagrand, O., 1997. Assimilation of observations, an introduction. *J. Meteo. Soc. Japan Series 2*, **75**, 81–99.

Tosi, N., Stein, C., Noack, L., HÃŒttig, C., MaierovÃ¡, P., Samuel, H., Davies, D.R., Wilson, C.R., Kramer, S.C., Thieulot, C., Glerum, A., Fraters, M., Spakman, W., Rozel, A., and Tackley, P.J., 2015. A community benchmark for viscoplastic thermal convection in a 2-D square box. *Geochem. Geophys. Geosys.*, **16**, 2175–2196.

Utke, J., Hascoët, L., Heimbach, P., Hill, C., Hovland, P., and Naumann, U., 2009. Toward adjoinable MPI. In *Proceedings of the 10th IEEE International Workshop on Parallel and Distributed Scientific and Engineering Computing, PDSEC-09*.

Vigny, C., Ricard, Y., and Froidevaux, C., (1991). The driving mechanism of plate tectonics. *Tectonophys.*, **187**, 345–360.

Walther, A. and Griewank, A., 2012. Getting started with adol-c. In *Combinatorial Scientific Computing*, chap. 7, pp. 181–202, eds Naumann, U. and Schenk, O., Chapman-Hall CRC Computational Science.

Worthen, J., Stadler, G., Petra, N., Gurnis, M. and Ghattas, O., 2014. Towards adjoint-based inversion for rheological parameters in nonlinear viscous mantle flow. *Phys. Earth. and Planet. Int.*, **234**, 23–34.

Xie, S. and Tackley, P. J., 2004. Evolution of U-Pb and Sm-Nd systems in numerical models of mantle convection *J. Geophys. Res.*, **109**, B11204.

Zhong, S., Zuber, M.T., Moresi, L. and Gurnis, M., 2000. Role of temperature-dependent viscosity and surface plates in spherical shell models of mantle convection. *J. Geophys. Res.*, **105**, 11063–11082.

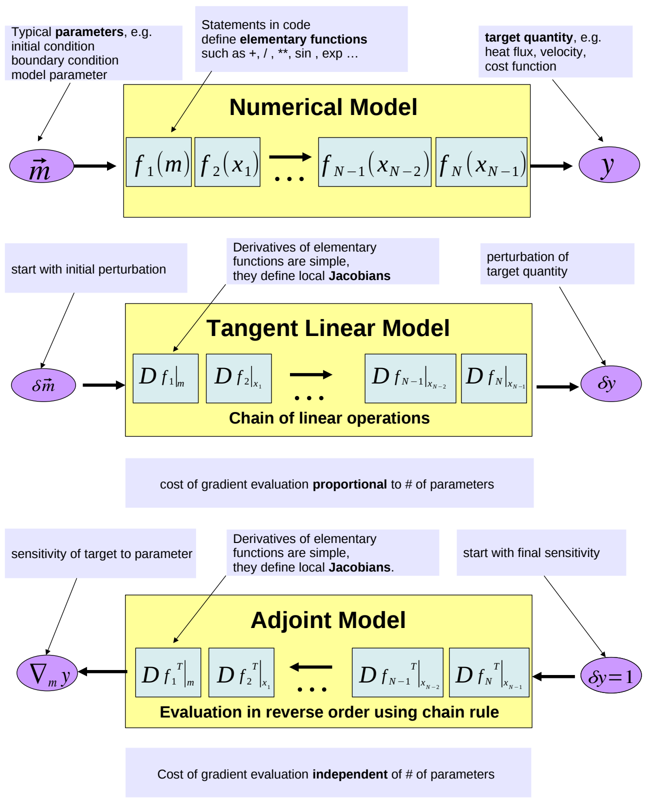

Figure 1. Top: diagram of operations for the forward numerical model to differentiate. Centre: diagram of operations differentiated in forward mode, corresponding to the tangent-linear code. Bottom: diagram of operation in reverse mode, corresponding to the adjoint code.

747 This paper has been produced using the Blackwell Scientific Publications GJI LaTeX2e class file.

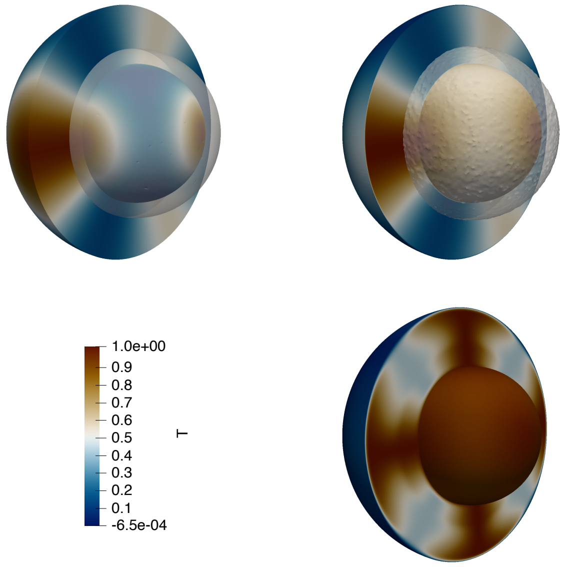

Figure 2. Setup for the gradient test of the automatically generated adjoint code 1. Top left: Initial condition (lateral spherical harmonic degree 3); Top right: final temperature field and isosurface showing the top of the dense layer. Bottom image: targeted temperature field after 10 time steps.

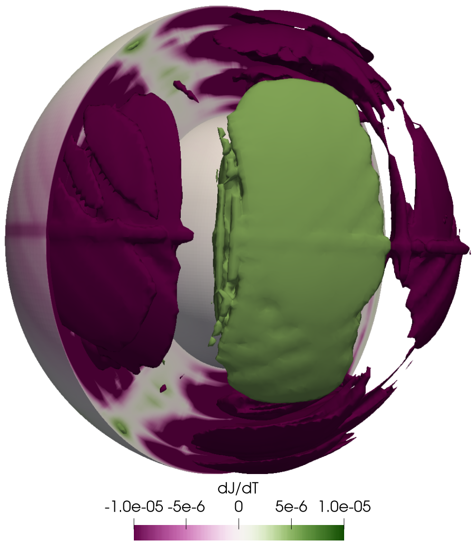

Figure 3. Volume section of the local sensitivity field $d\mathcal{J}^T/dT$. The color is saturated to identify positive values (the initial local temperature should be increased to increase the cost function) and negative values (the initial local temperature should be decreased to increase the cost function).

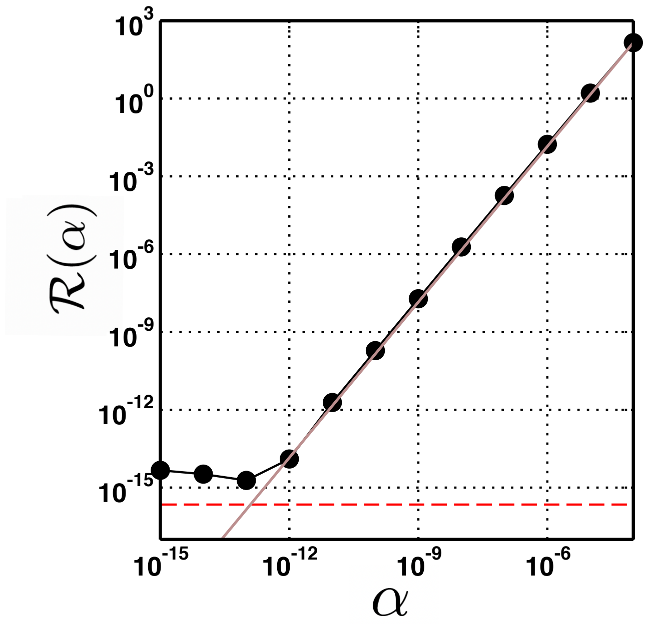

Figure 4. Gradient test for the benchmarking adjoint code 1, showing the relationship between α and $\mathcal{R}(\alpha)$. Computed values are in black circles. The red horizontal dashed line corresponds to the value of machine ε. The brown line corresponds to α^2 that $\mathcal{R}(\alpha)$ has to match to pass successfully the gradient test.

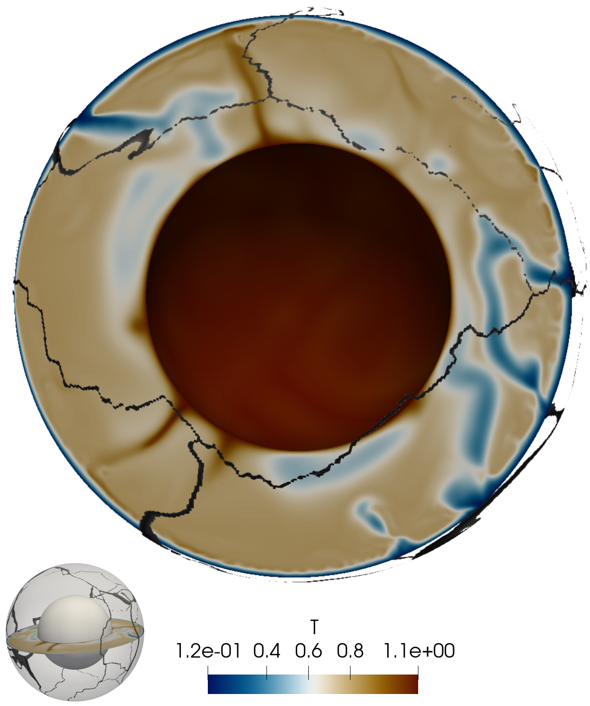

Figure 5. Cross section of the non-dimensional nudged temperature guess. The location of the cross section is shown on the small globe and crosses Northern Chile and the Philippines. Plate boundaries are represented in black. The top of the model shows the South Atlantic ridge. The slab on the left shows subduction below South America. Slabs on the right correspond to Asia-Pacific subduction system in a 3D system.

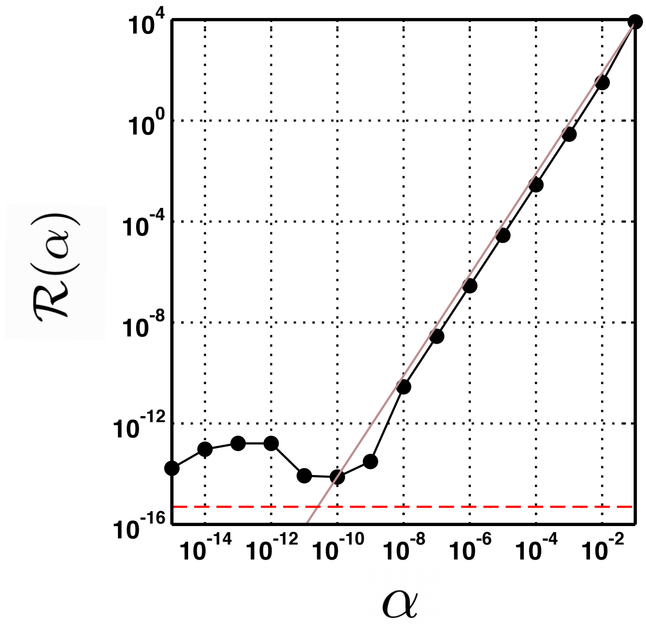

Figure 6. Gradient test for the 'nudged' case, showing the relationship between α and $\mathcal{R}(\alpha)$. Computed values are in black circles. The red horizontal dashed line corresponds to the value of machine ε. The brown line corresponds to α^2 that $\mathcal{R}(\alpha)$ has to match to pass successfully the gradient test.

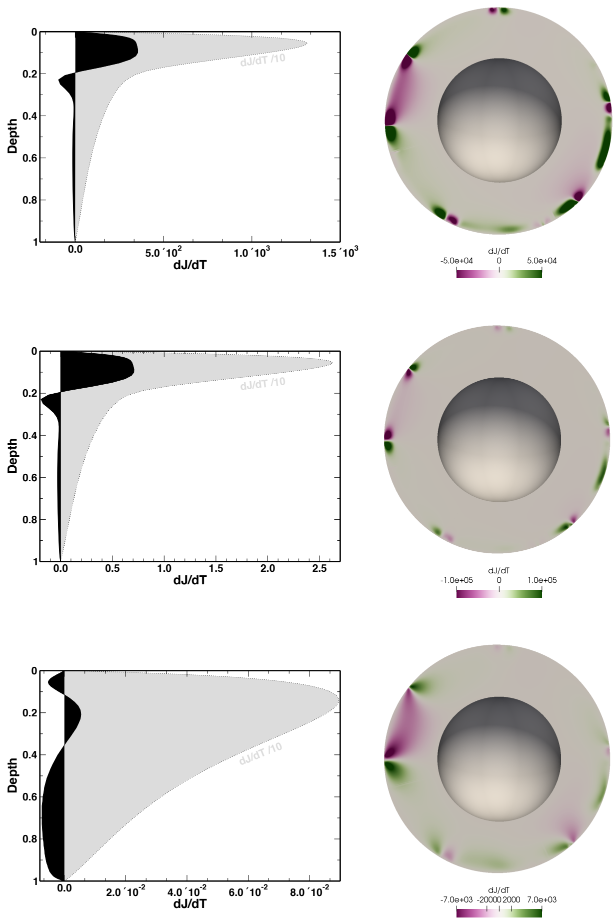

Figure 7. Left column: sensitivity field $d\mathcal{J}^v/dT$ as a function of depth (laterally averaged in black and root-mean square value in gray). Right column: volume section of the local sensitivity field $d\mathcal{J}^v/dT$. The section is identical to that of Fig5. Top row: reference model. Middle row: high yield stress model. Bottom row: model without a viscosity jump. Positive values mean that the local temperature should be increased to increase the cost function and negative values suggest the local temperature should be decreased to increase the cost function.

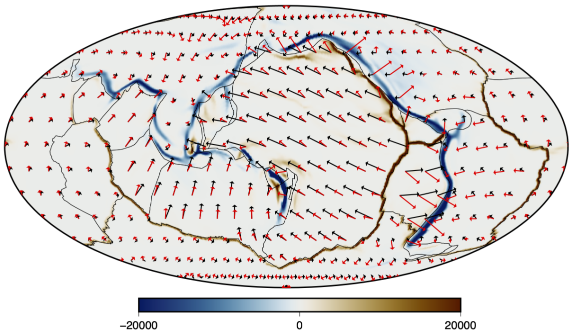

Figure 8. Surface kinematics of the convection model (forward model solving for the velocity field in response to the 3D temperature distribution) vs. plate reconstruction model. Computed velocities are in red together with predicted non-dimensional divergence in colors. Velocities and plate boundaries for the plate reconstruction model are represented in black.

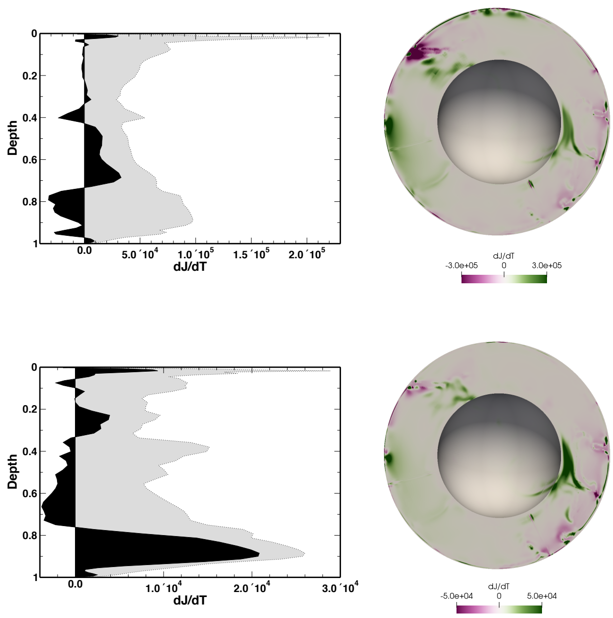

Figure 9. Left column: sensitivity field $d\mathcal{J}^v/dT$ as a function of depth (laterally averaged in black and root-mean square value in gray). Right column: volume section of the local sensitivity field $d\mathcal{J}^v/dT$. The section is identical to that of Fig5. Top row: reference model. Bottom row: model without viscosity jump. Positive values mean that the local temperature should be increased to increase the cost function and negative values suggest the local temperature should be decreased to increase the cost function.